



Optimization of process parameters influencing the sustainable construction of iron oxide nanoparticles by a novel tropical wetlands *Streptomyces* spp.

Patricia Jayshree Jacob ^{a, d}, Mas Jaffri Masarudin ^{a, b, c, *}, Mohd Zobir Hussein ^c, Raha Abdul Rahim ^a

^a Department of Cell and Molecular Biology, Faculty of Biotechnology and Biomolecular Sciences, Universiti Putra Malaysia, 43400, UPM Serdang, Selangor, Malaysia

^b Institute of Biosciences, Universiti Putra Malaysia, 43400, UPM Serdang, Selangor, Malaysia

^c Institute of Advanced Technology, Universiti Putra Malaysia, 43400, UPM Serdang, Selangor, Malaysia

^d Department of Biosciences, Nilai University, Persiaran University, 71800, Negeri Sembilan, Malaysia

ARTICLE INFO

Article history:

Received 16 August 2018

Received in revised form

27 May 2019

Accepted 29 May 2019

Available online 1 June 2019

Keywords:

Melanin induced

Bionanoparticles

Optimization

Size

Polydispersity

Temperature

Biomass

Precursor concentration

Reaction kinetics

Keywords:

Iron oxide nanoparticles

External parameters

Microbial mediated

RSM

OVAT analysis

ABSTRACT

A *Streptomyces* strain isolated from the soil sediments of tropical freshwater wetlands in Malaysia demonstrated promising attributes to be developed into a versatile microbial nanofactory for the sustainable synthesis of ferric oxide nanoparticles (IONP). Process parameters such as temperature, ferric salt precursor concentration, cell free extract (CFE) concentration and biomass harvesting times are serious players in the extracellular generation of metallic nanoparticles. A statistical approach using One-Variable-At-A-Time (OVAT) Analysis followed by Response Surface Methodology (RSM) was employed towards the optimization of the microbial bioprocess and modulation of nanoparticle size dimensions. OVAT revealed that IONP production increased with increasing temperature, precursor concentration, harvesting time and CFE concentration with highest yield at 65 °C, 2 mM precursor concentration, 68 h harvesting time and 100% CFE concentration. A detailed statistical analysis using RSM (RSM) showed significantly strong negative interactive effects between temperature and CFE concentration ($p = 0.0037$), temperature and precursor concentration ($p = 0.0093$) and mild interactive effects between CFE and precursor concentration ($p = 0.0301$). Taking into account the interactive influence of these variables, numerical analysis using RSM proposed that for optimal generation of microbial mediated IONP, a CFE concentration of 55.58%, temperature of 55.75 °C and precursor concentration of 2.46 mM $\text{FeCl}_3 \cdot 6\text{H}_2\text{O}$ would be required.

© 2019 Elsevier Ltd. All rights reserved.

1. Introduction

Nanoscale iron particles as compounds of oxides, sulfides and hydroxides have emerged to prominence in recent years due to their multi-faceted application potential in diverse fields. The derivatives of nanoscale ferric particles, namely magnetite (Fe_3O_4),

maghemite ($\gamma\text{-Fe}_2\text{O}_3$), hematite ($\alpha\text{-Fe}_2\text{O}_3$), griegite (FeS) and zero-valent iron oxides have been widely explored for their role in biomedicine (Couto et al., 2015), electrochemical sensing (Teymourian et al., 2013) and groundwater remediation (Fenglian, Fu et al., 2014). At nanoscale dimensions, iron oxides have are found to possess unique magnetic properties or superparamagnetism (Wahajuddin, and Arora, 2012) where robust magnetic saturation was observed with the application of an external magnetic field, and a sequential loss of this magnetic property when the external magnetic field was removed. This phenomenon forms the basis towards the application of iron based nanoparticles as contrast

* Corresponding author. Department of Cell and Molecular Biology, Faculty of Biotechnology and Biomolecular Sciences, Universiti Putra Malaysia, 43400, UPM Serdang, Selangor, Malaysia.

E-mail address: masjaffri@upm.edu.my (M.J. Masarudin).

enhancement agents for MRI imaging (Shen et al., 2017), targeted-cell drug delivery (Dong et al., 2015), magnetic tape recording (Ohkoshi, et al., 2016) and the destruction of malignant tumors through magnetic hyperthermia (Abenojar et al., 2016).

However, IONPs still remain limited in widespread use as the current methods of synthesis necessitate surmounting investment in energy and equipment, a specialized labor force to undertake meticulous protocols and the nagging fear of environmental repercussions (Saif et al., 2016). Contingent to these drawbacks, continual research has curtailed to a wide exploration of biological-based systems derived from plants, bacteria, fungi and algae systems as a promising alternative. Here, biomaterials such as enzymes, pigments or secondary metabolites (Adelere and Lateef, 2016) function as reducing, stabilizing or capping agents in the fabrication of IONPs from metal salt precursors. Bio-based synthesis integrates the principles of green chemistry, has minimal environmental discharge, cost effective investment, ease of scale-up and simple, straightforward methodology.

Certain microorganisms possess the cellular machinery to detoxify heavy metal ions (Oves et al., 2016) in their environment by reducing them to less potent forms. Bio-reduction of metallic ions forms the basis for microbial biosynthesis of nanoparticles using the extracellular route. In this process, biomolecules are released to the extracellular matrix to breakdown metallic ions in aqueous solutions and form nano-sized particles (Adelere and Lateef, 2016). Microbial enzymes such as reductases, amylases (Ahmad et al., 2015) or keratinases (Lateef et al., 2015) have the potential to catalyze the formation of metallic nanoparticles and generate stabilizers or capping agents in the process. Similarly, microbial pigments such as cochineal (Kumar et al., 2016), melanin (Apte et al., 2013) and fucoxanthin (Jayashree et al., 2015) have effectively reduced metallic ions in the green synthesis of Au, Ag and Se metallic nanoparticles.

We reported earlier the isolation of MS2, a prokaryote from the *Streptomyces* genera, from the riverbed sediments originating from the tropical freshwater wetlands in the West Coast of Peninsular Malaysia (Jacob et al., 2017) and the characterization of IONP generated in its extracellular matrix with the addition of a Fe salt precursor. Compared to conventional synthesis protocols, this microbial bioprocess is undoubtedly a cleaner method in IONP generation as it negates high energy and equipment cost as required in laser pyrolysis, electron beam lithography and high energy ball milling (Lin and Samia, 2006) and complies with the underlying principles of green technology by not discharging hazardous waste or using potent solvents, stabilizers or capping agents as required in conventional chemical synthesis methods such as co-precipitation, microemulsion and electrochemical decomposition (Wu et al., 2008). Although microbial bioprocesses to generate metallic nanoparticles have always been sidelined due to its low rate of production, IONP generation was observed in this MS2 biosystem within 10–30 min of incubation at 28 °C or room temperature, making it a bioprocess that warrants attention and should be further pursued for commercial production.

In a microbial biosystem, process parameters such as temperature, precursor concentration, pH and biocatalyst concentration have to be modulated for optimal rate of nucleation and in designing size specific, mono dispersed nanoparticles. In this investigation, we report the influence of temperature, pH, precursor and biomass concentration on the reaction kinetics and rate of IONP generation as reflected in the absorbance using the UV–Vis Spectrophotometer. The manipulation of these parameters on the size and polydispersity of these IONPs is surveyed using Dynamic Light Scattering (DLS) as recorded on the Nanosizer.

2. Experimental

2.1. Instruments and reagents

Growth and maintenance of *Streptomyces* sp MS2 on Nutrient Agar (NA) (5 g/L peptic digest of animal tissue, NaCl 5 g/L, Beef extract 1.5 g/L, Yeast extract 1.5 g/L and Agar 15 g/L) and Nutrient Broth (NB) (peptones 15 g/L, yeast extract 3 g/L, NaCl 6 g/L, D (+)-Glucose 1 g/L) purchased from Himedia, India. Iron (III) chloride hexahydrate, $\text{FeCl}_3 \cdot 6\text{H}_2\text{O}$, (QRec, Italy) was used as the ferric salt precursor. Characterization of the IONPs were carried out using UV/Vis Spectrophotometer, HumanCorp (X-ma 1000) and the Nano Sizer (Malvern Nano S).

2.2. Extracellular biosynthesis of IONP by tropical *Streptomyces* sp MS2

Streptomyces sp MS2, was maintained on L-tyrosine (2.5%) supplemented (NA) slants. A fresh inoculum of MS2 was transferred into 30 ml L-tyrosine (2.5%) supplemented (NB) and incubated at room temperature (28 °C) with shaking at 150 rpm for 24 h – 48 h. Following this, the liquid culture was centrifuged (5000 rpm, 15 min) and the supernatant transferred to fresh Falcon tubes. For the production of IONP, an equal volume of 2.0 mM $\text{FeCl}_3 \cdot 6\text{H}_2\text{O}$ was added to the supernatant and the color change observed. IONP was harvested by spinning the supernatant with the ferric salt precursor at 15000 rpm for 20–30 min and dried over a period of 3 days under room temperature (28 °C). A growth curve of the bacteria was plotted over a period of 18–55 h together with the bio-production of IONP using CFE harvested at different time periods along the growth curve to study the peak production of IONPs according to the growth curve.

Characterization of biosynthesized IONPs was carried out using UV–visible spectrophotometer (X-Ma 1000, HumanCorp, Korea), Field Emission Scanning Electron Microscope (FESEM) with X-ray Energy.

Dispersive Spectrometer (EDS) and Transmission Electron Microscopy (TEM) to verify the generation of IONP and to study its morphology, size and elemental composition.

2.3. The influence of temperature, precursor concentration and harvesting time on IONP formation using the OVAT method

To evaluate the influence of temperature, precursor concentration and harvesting time on the reaction kinetics, size and polydispersity of IONP, the reaction was carried out under different temperatures (28 °C, 37 °C and 65 °C), precursor concentration (0.5 mM, 1.0 mM and 2.0 mM) and CFE biomass harvested after 22 h, 44 h and 52 h incubation. Parameters that were kept constant included ferric salt precursor ($\text{FeCl}_3 \cdot 6\text{H}_2\text{O}$) pH (pH 6), humidity (98%) and rotation speed (150 rpm) were maintained as a constant. The ranges used for each variable in the OVAT analysis were based on observations made during preliminary runs which demonstrated optimal IONP production within these range of temperature, CFE harvesting times and precursor concentration. Characterization of the IONP's was carried out using the UV Spectrophotometer at a wavelength range of 250–600 nm.

2.4. The effect of different concentrations of CFEs, temperature, and precursor concentration on the kinetics of the formation of IONP

The kinetics of IONP formation was studied using different CFE concentrations (10%, 25%, 50% and 100%), temperature (26 °C, 37 °C and 65 °C) and ferric salt concentration (0.5 mM, 1.0 mM, 1.5 mM and 2.0 mM). Absorbance at 400 nm was recorded for the reaction

mixture after 1 h, 3 h, 5 h and 24 h incubation.

2.5. The effect of temperature, precursor concentration, harvesting at different growth periods and CFE concentration on the size distribution and polydispersity of the bio-generated IONP

The reaction mixture containing equal volume CFE and ferric salt ions were adjusted to different temperatures (28 °C, 37 °C and 65 °C), precursor concentrations (0.5 mM, 1.0 mM and 2.0 mM), CFE concentrations (25%, 50% and 100%) and biomass harvesting times (20 h, 25 h, 44 h and 52 h). The IONPs formed were harvested through centrifugation at 20000 rpm for 20 min and dissolved in sterile distilled water before analyzing it using a Nanosizer for particle size and polydispersity.

2.6. Optimization of external parameters using RSM

A statistical modeling approach using RSM (RSM) was carried out to determine the influence of selected parameters on IONP generation rate and yield. The Design Expert Version 6.0.7 (Stat-Ease, Inc., Minneapolis, USA) was used in the design of experiments and graphical analysis of data. The Box-Behnken Design (BBD) in RSM was used to optimize the selected parameters and probe the interactive effect of 3 independent variables- A-CFE concentration, B-temperature and C-precursor concentration-at 3 levels - low (–), medium (0) and high (+) levels with the response being IONP yield reflected in the OD₄₀₀ reading on the UV–Vis Spectrophotometer. The Box-Behnken Design is a 3-level rotatable composite design which allows the testing of each variable at different levels several times. Compared to other factorial designs, it requires fewer experimental runs based on fewer design points but does not compromise on its reliability to predict experimental outcomes. Additionally, all points fall within the boundaries of manageable operations and avoids manipulation of variables under unrealistic conditions. The number of experiments required for the Box-Behnken design can be calculated as:

$N = k^2 + k + c_p$, where k is the number of variables and c_p is the replicate number of the central points.

In optimization, the experiments were conducted out as stipulated in the design matrix and an evaluation of the regression coefficients in the mathematical model was made using the response results of the experiment. With this model, interaction between parameters could be statistically determined and the optimum conditions for IONP production could be predicted. Table 1 depicts the design variables with low –1 and high +1 levels for the 3 independent variables were A [50 and 100%], B [30 and 60 °C] and C

[0.5 and 2.5 mM] and central values being A-75%, B-45 °C and C-1.5 mM respectively.

A Box-Behnken design matrix with a total of 17 runs was constructed using the Design Expert software (as shown in Table 2) to optimize the 3 independent variables with the range and levels determined from the results of the OVAT analysis. Analysis of data using RSM requires a prediction model to determine the response between independent variables on IONP yield as manifested in the graph curvature and to detect interactions between independent variables for process optimization to obtain maximum IONP yield. The relationship between the independent variables to the response was fitted to a second-order quadratic polynomial equation as shown below with the independent variables A, B and C coded as X1, X2 and X3 respectively and Y showing the response:

The model used for statistical predictions were assessed using the Fisher's *F*-test and model significance was evaluated using the analysis of variance (ANOVA) and a multiple regression analysis R^2 was carried out to determine model fitness to the responses obtained.

3. Results and discussion

3.1. Extracellular biosynthesis of IONP by tropical *Streptomyces* sp MS2

MS2 is a cream colored *Streptomyces* strain isolated from tropical riverbed sediments of Peninsular Malaysia which produces diffusible brownish black pigmentation after 26–28 h incubation in L-tyrosine supplemented NA (Jacob et al., 2017). When an equal volume of ferric ion salts, (2 mM FeCl₃·6H₂O) are added to the MS2 CFE, a rapid color change is observed from brown to black, indicating the formation of iron oxide nanoparticles (Jacob et al., 2017).

In microbial generation of IONP, a bio-reducing agent, in the form of an enzyme, pigment or secondary metabolite, is necessary to reduce ferric ions to form iron particles that participate in the nucleation of IONP. Microorganisms such as *Legionella pneumophila* (Zheng et al., 2013) and *Cryptococcus neoformans* (Wang et al., 1995) have demonstrated that secreted extracellular melanin mediates the reduction of ferric ions (Turick et al., 2002). In this investigation, a brownish melanoid pigment, released by the bacteria MS2 after 26 h incubation in L-tyrosinase supplemented media, is suspected to be the bio-reducing agent. This melanoid pigment was precipitated in 5N HCl and redissolved in water. Preliminary biochemical investigation as recorded in Table 1 below suggests that this pigment was melanin. As a control, equal volume of the precursor is added to MS2 supernatant harvested from culture grown in NB without L-tyrosine. No color change is observed upon addition of the precursor. Although this observation supports the hypothesis of melanin as the bio-reducing agent required to induce IONP generation, further investigation is necessary for confirmation.

Fig. 1a shows the growth curve of MS2 plotted over a period of 18–56 h incubation, compared with the rate of IONP production at different harvesting periods along the growth curve. From this graph, MS2 experiences exponential growth at a period between 28 and 46 h before reaching the stationary phase. IONP production in the exponential phase progresses slowly (gradient = 0.0277)

Table 1

Experimental range with the actual and coded values for the 3 independent variables.

Variable	Name	Unit	Actual			Coded		
			High	Medium	Low	High	Medium	Low
A	CFE	%	100	75	50	+1	0	–1
B	Temperature	°C	60	45	30	+1	0	–1
C	Concentration	mM	2.5	1.5	0.5	+1	0	–1

Table 2

Preliminary biochemical characterization of melanin like pigment.

Solubility	1M KOH	1M NaOH	1M HCl	Ethanol	H ₂ O	Ether
	Insoluble	Insoluble	Soluble	Insoluble	Insoluble	Insoluble
iochemical Tests	H₂O₂ Decolorization	NaHClO₃	AgNO₃ Precipitation	Phenol	KMnO₄ Oxidized	K₂Cr₂O₇

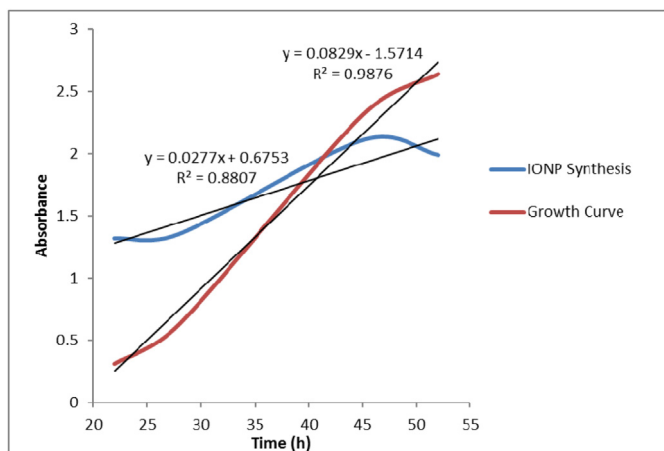


Fig. 1a. MS2 growth curve against production of IONP by extracellular CFE harvested at different periods corresponding to the growth curve.

compared to the growth rate of the bacteria (gradient = 0.0829). In the exponential phase, the rapid increase in biomass corresponds to the increased production of melanin, which when accumulated in the CFE at different periods of harvesting, correspond to the increasing rate of IONP generation. However, as the production of IONPs increase in a fixed reaction volume, they are brought to close proximity with each other, increasing the attraction force and causing the agglomeration of IONP molecules. When the cell growth rate tapers off after 48–52 h, IONP production rate decline, suggesting that the increase in melanin production (which reaches a maximum after 52 h), does not increase the IONP generation rate after a certain limit as all ferric ions present in the reaction mixture have been reduced to form IONP.

Characterization of MS2 generated IONP was carried out using FESEM-EDX, TEM and UV–Vis spectrophotometry. Fig. 1 (b) shows the (i) UV absorbance spectra, (ii) FESEM and (iii) TEM results of the microbial generated IONPs together with its (iv) EDS profile. From the UV absorbance spectra in Fig. 1b (i), it can be shown that the absorbance peak of the biosynthesized nanoparticles was in the wavelength range of 380–400 nm. This is consistent with the UV absorbance peak of green synthesized IONPs as reported by Turkahia, B. et al. (2018) and Amutha, S. and Sridhar, S. (2018), postulating the formation of IONPs in the extracellular matrix of MS2. The morphology of these IONPs are further visualized in the FESEM images in Fig. 1 (b) (ii), depicting agglomerated octahedral structures in a size range between 38 and 62 nm. The HrTEM images in Fig. 1 (b) (iii) show clear crystal lattice fringes confirming the formation of nanocrystals surrounded by an amorphous layer which depicts nanoparticles prior to nucleation. The elemental composition of the nanostructures depicted in the FESEM and HrTEM images were illustrated in the EDS spectra where Fe peaks were shown at 0.7 keV and 6.4 keV, consistent to IONPs generated using green synthesis by Ozgür, M.E. et al. (2018). Detailed characterization of this IONPs have been discussed in an earlier paper by Jacob, P. et al. (2017).

3.2. The influence of CFE harvesting time, temperature and ferric ion salt concentration on melanin aided IONP formation

Fig. 2 depicts the UV spectra at different precursor ferric ion concentrations, CFE concentrations based on different harvesting times at different bacterial growth periods and temperature. Absorption intensity increases corresponding to the growth periods of the bacteria harvested after 28 h, 45 h, 50 h and 68 h of incubation. The highest absorption intensity is recorded for CFE from cells harvested after 68 h of incubation. Increased bacterial density

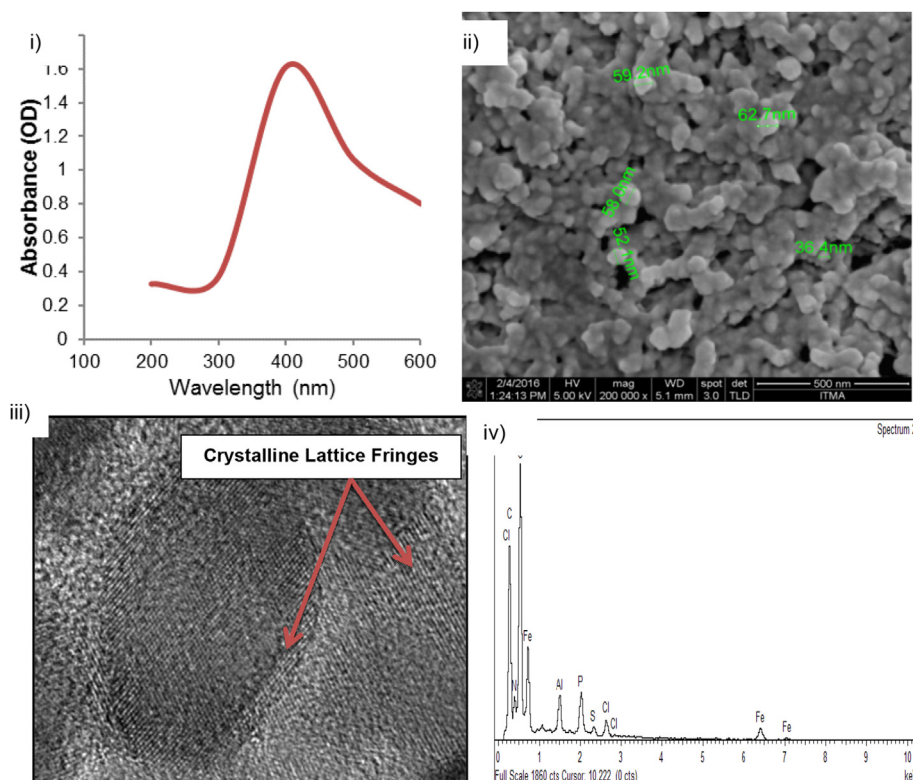


Fig. 1b. (i) UV absorbance spectra, (ii) FESEM image, (iii) Crystal lattice structure and (iv) EDX of MS2 mediated IONPs.

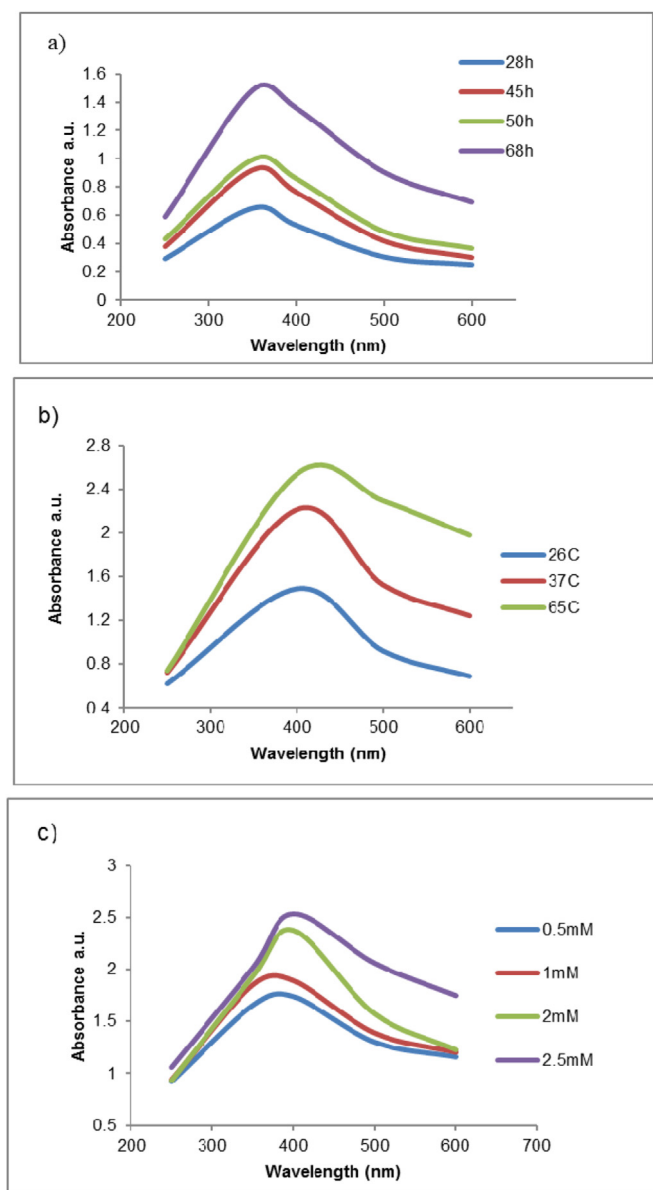


Fig. 2. UV absorption spectra of IONPs formation over a wavelength range of 250–600 nm for (a) CFE harvested after 28 h, 45 h, 50 h and 68 h incubation (b) incubation temperatures of 26 °C, 37 °C and 65 °C and (c) 0.5 mM, 1.0 mM, 2.0 mM and 2.5 mM of iron salt precursor.

progressing with incubation time inevitably leads to the increase in the bio-reducing agent, presumably melanin, in the CFE. Increase in melanin concentration leads to increased production of IONP as indicated by the higher peak at 68 h. Fig. 2b shows the effects of temperature (26 °C, 37 °C and 65 °C) on the formation of IONPs, with the highest intensity recorded at 65 °C. A clumping of IONPs was observed in the reaction mixture which had to be separated by filtration at this temperature. Therefore, the higher absorbance reading could be attributed to the agglomeration of the IONPs at 65 °C, causing the emission in the UV spectra to detect the agglomeration as single molecules. From Fig. 2b, a marked increase of IONP production was observed from an incubation temperature of 26 °C–37 °C as compared to 37 °C–65 °C with a decrease in peak sharpness indicating polydispersity. This is a preliminary indication that IONP production rate increases from an incubation temperature of 26 °C–37 °C but slowly reaches an equilibrium closer to

65 °C. It was also evident that higher temperatures did not effect nanoparticle stability or degrade the biomolecule acting as the template for IONP production. Fig. 2c demonstrates that increasing the precursor concentration from 0.5 mM to 2.0 mM corresponds to an increase in IONP production with a sharp increase indicated from 1.0 mM to 2.0 mM. The sharpest peak is recorded at a precursor concentration of 2.0 mM, suggesting monodispersity of the IONPs produced. At 2.5 mM, although an increase is reported, the curve loses its sharp peak, implying the polydispersed nature and possible agglomeration of the nanoparticles generated.

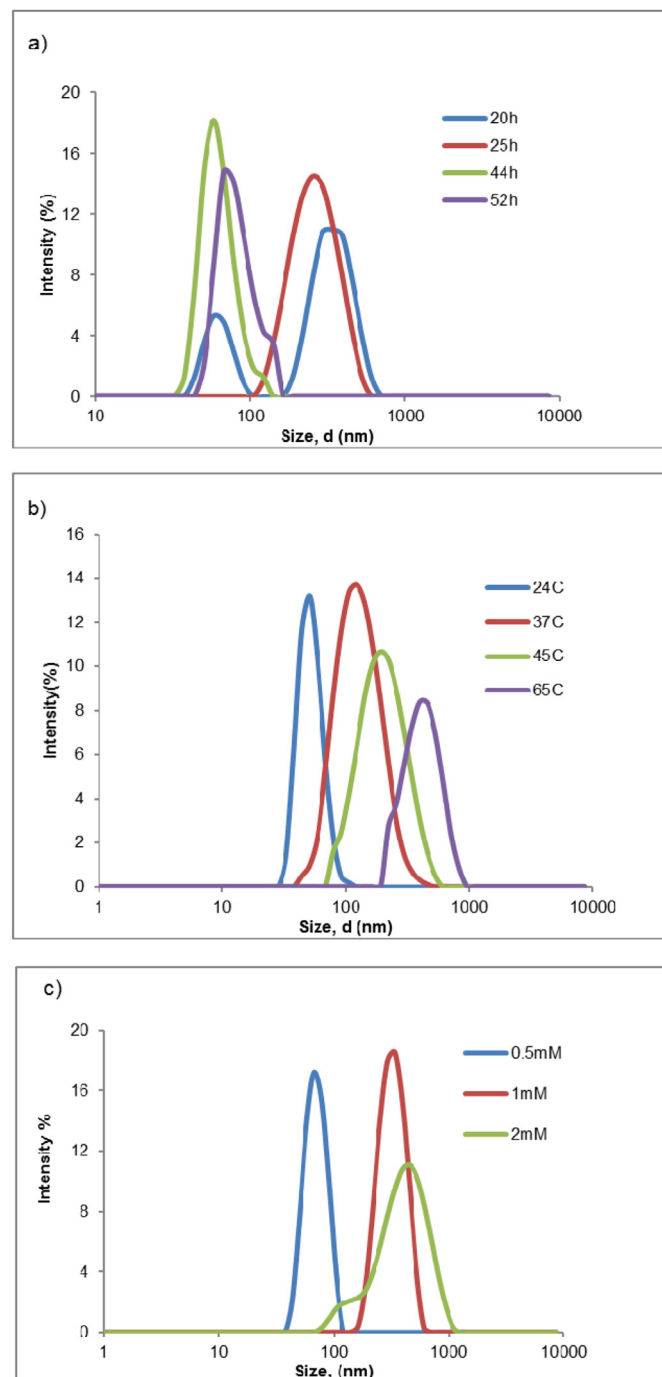


Fig. 3. Particle size distribution of IONP at different a) harvesting periods of CFE, b) reaction temperature and c) ferric ion salt concentration.

3.3. Influence of bacterial harvesting periods, reaction temperature, concentration of iron salt precursor and concentration of extracellular matrix and on IONP size distribution and polydispersity

Fig. 3a depicts the particle size distribution of the IONPs generated from CFEs harvested after 20, 25, 44 and 53 h. From this chart, the size distribution of the particles show a decrease of size for CFE harvested progressively from 20 to 44 h. This coincides with the exponential growth phase of the bacteria as depicted in Fig. 1 which postulates that biocatalyst production increases rapidly during the exponential growth phase, causing rapid breakdown of ferric ions to generate IONPs of smaller size distribution. However, at 53 h, during which time bacterial growth reaches the stationary phase, the generation of biocatalyst reaches equilibrium and an accumulation of IONPs at close proximity during this stage causes agglomeration as shown by the increase in particle size with CFE harvested at this time. Additionally, melanin, the biocatalyst, could have reached its maximum production rate prior to the stationary phase and accumulation of secondary metabolites could interfere with the bio-reduction of IONPs.

Reaction temperature can affect the reduction of Fe^{3+} ions, nucleation of IONP clusters and particle aggregation rate. However, the affinity of melanin for metallic ions and its ability to rapidly reduce or chelate these ions are not significantly affected by minor changes in temperature. Fig. 3b shows an increasing pattern in nanoparticle size distribution with an increase in temperature. Smaller (52.51 nm) nanoparticles with higher monodispersity (as observed by peak sharpness) was observed for reaction temperatures at 24 °C (room temperature). With the increase in reaction temperature, larger particles were obtained. At 37 °C and 45 °C,

nanoparticle size distribution showed a peak at 122.4 nm and 190.1 nm respectively. Larger particles and decreasing peak sharpness at 65 °C could be caused by a drastic increase in particle aggregation rate caused by the high reaction kinetics of increasing reaction temperature.

Fig. 3c shows that an increase in precursor concentration shows a positive correlation to particle size distribution. Nanoparticle formation is usually the result of 3 main processes: particle nucleation, nuclei growth to primary particles and secondary changes resulting in agglomeration. The number of particles participating in nucleation is dependent on the availability of Fe^{3+} supplied by the precursor. This explains why at lower concentration, particle size is lower compared to higher concentrations. At concentrations of precursor beyond 2 mM, particle aggregation becomes prominent, causing an increase in particle size dimensions. It is postulated that precursor to biocatalyst ratio is a major player in determining the outcome of nanoparticle size and rate of nanoparticle formation.

Fig. 4a shows the correlation between the polydispersity index of the IONP generated from *Streptomyces* CFE harvested after 20, 28, 44 and 52 h of incubation. The polydispersity index decline for IONPs prepared from CFEs harvested after 20–44 h of incubation and stabilizes after this point. This correlates to Fig. 3a) where the size distribution of IONPs prepared from CFE harvested after 20 h incubation shows multiple peaks indicating high polydispersity. The peaks for size distribution of IONPs prepared from CFEs harvested at 44 h and 52 h however, were more mono-dispersed as depicted by the narrow peaks in Fig. 3a) which coincides with the PDI depicted in Fig. 4a). This could be a result of insufficient levels of biocatalyst needed to break down ferric ions in aqueous solution to produce IONPs. This resulted in a polydispersed mixture of IONPs

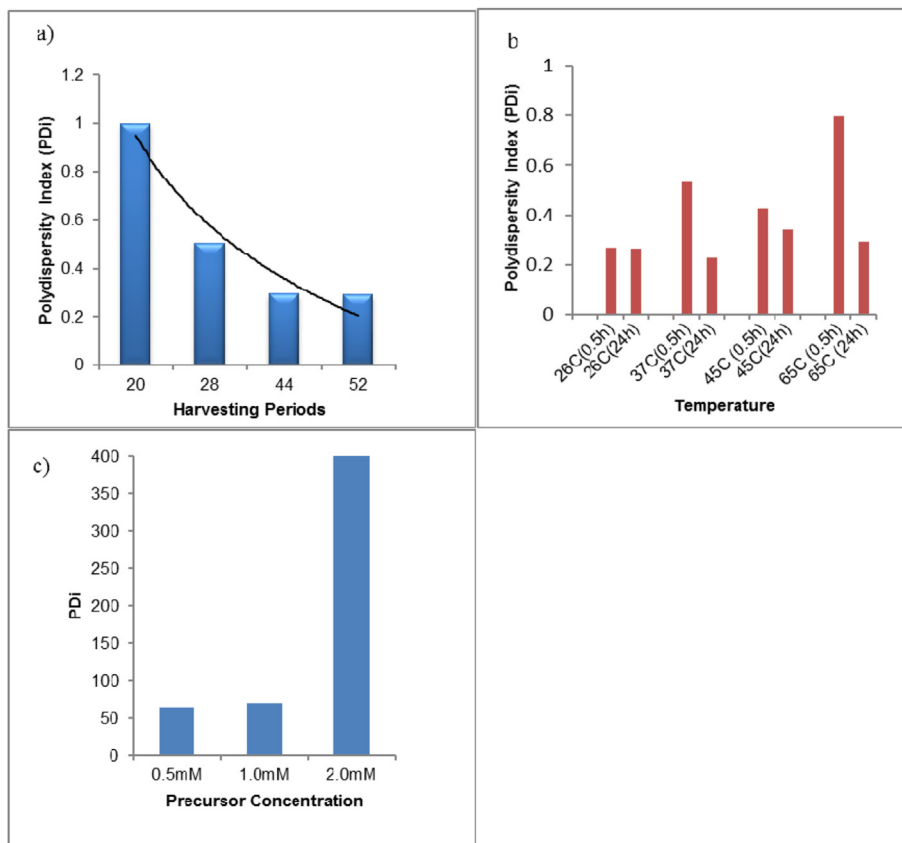


Fig. 4. Polydispersity Index (PDI) of IONP at different a) harvesting periods of CFE, b) reaction temperature and c) ferric ion salt concentration.

made up of nanoparticle aggregates and smaller IONPs with insufficient nucleation. However, CFE collected after 44 h of incubation has reached the maximum production of biocatalyst which is sufficient to reduce ferric ions and induce nucleation of IONPs with uniform size distribution.

Fig. 4b) shows the PDI as compared to reaction temperature after 30 min and 24 h incubation at 24 °C, 37 °C, 45 °C and 65 °C. From this chart, PDI increases with increasing incubation temperature for the 30-min incubation period but declines as settles to a lower PDI after 24 h incubation. The PDI is lowest at 24 °C which coincides with Fig. 3b) depicting narrow size distribution as illustrated by the sharpest peak at 24 °C, which is room temperature. This interesting feature suggests that IONPs with narrow size

distribution could be produced from this bioprocess without the need of excess energy or heating. Fig. 4c) depicts the correlation between PDI and iron salt precursor concentration. No significant change in PDI is displayed using iron salt precursor at 0.5 mM and 1.0 mM concentrations but a rise in PDI is observed for precursor concentration at 2.0 mM. A rise in precursor concentration at this juncture without altering the concentration of biocatalyst could lead to production of unevenly sized IONPs caused by insufficient biocatalyst to reduce ferric ions in solution to induce IONP nucleation. This could also lead to an aggregation of excess ferric ions in solution provided by the high concentration of the precursor which causes larger, polydispersed IONPs, coinciding with the broad peaks observed in Fig. 3c for 2 mM precursor concentration.

3.4. Influence of CFE concentration, pH, temperature, and precursor concentration on IONP formation kinetics

Fig. 5 shows IONP formation kinetics at different (a) CFE concentrations, (b) temperature, (c) precursor concentrations and (d) pH. The biosynthesis of IONP goes through 3 main stages from particle seeding and nucleation, growth and phase transformation. A rapid rise to maximum absorbance value within the first 3 h is caused by reduction of ferric ions, nucleation and growth of IONPs (Rao, K.J. and Paria, S. 2014) which drops to a constant due to saturation and completion of the reduction reaction. This demonstrates that the biomass retention time in the bioreactor need not exceed 4 h for IONP formation. IONP concentration or amount is proportional to the absorbance at its peak wavelength of 350 nm and is affected by changes in temperature, pH, CFE concentration and ferric salt precursor concentration.

From Fig. 5a, it is observed that as the concentration of CFE decreases, there is a decrease in IONP production. This could be a result of the depletion of biocatalyst molecules at low CFE at low concentrations (10%), which halts the process of ferric ion reduction and nucleation. At 100% concentrations, the biocatalyst production is the highest and sufficient for ferric ion breakdown within the first 3 h of the reaction. Although at lower CFEs the time taken for IONP production is not significantly different, there is a decrease in the amount of IONP generated.

Fig. 5b shows that an increase in temperature leads to an increase in the amount of IONP generated but do not display any significant difference in the rate of IONP formation. At 26 °C, there

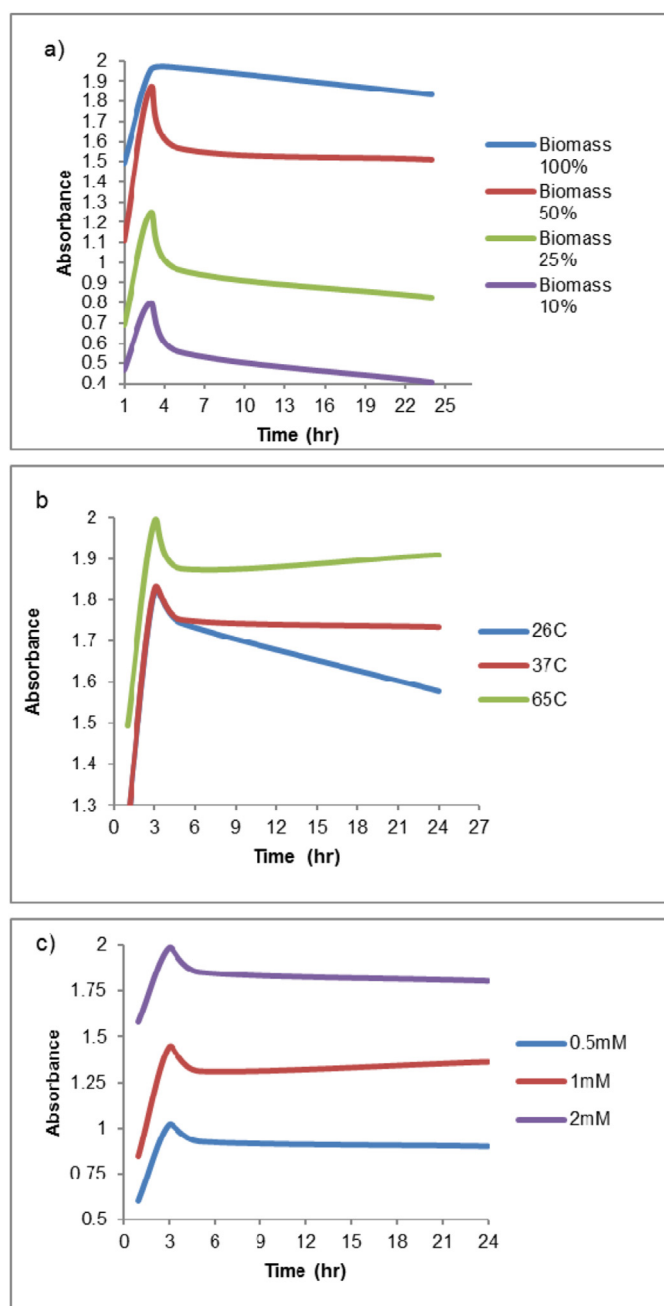
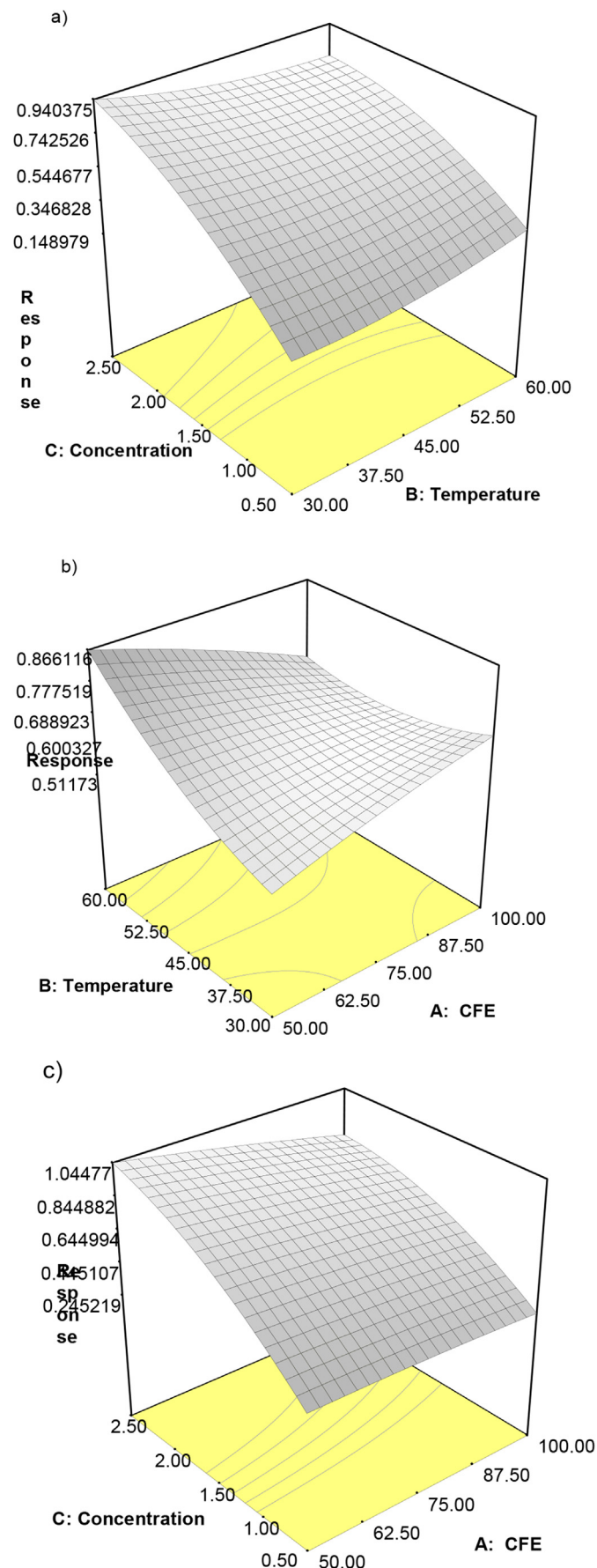


Fig. 5. Absorbance of IONP at different a)biomass concentrations b) reaction temperature and c) ferric ion salt concentration recorded after 1 h, 3 h, 5 h and 24 h incubation.

Table 3

Experimental design created using the BBD in the RSM model with the actual and predicted values.

Run	Independent Variable			Response (OD ₃₈₀)	
	A CFE (%)	B Temperature (°C)	C Concentration (mM)	Actual	Predicted
1	100	30.00	1.5	0.643	0.65
2	75	45.00	1.5	0.634	0.61
3	50	45.00	2.5	0.938	0.95
4	75	45.00	1.5	0.652	0.61
5	75	45.00	1.5	0.606	0.61
6	50	60.00	1.5	0.857	0.85
7	100	45.00	2.50	0.842	0.80
8	75	30.00	0.5	0.015	0.016
9	75	45.00	1.5	0.578	0.61
10	100	45.00	0.5	0.184	0.17
11	75	60.00	2.5	0.933	0.93
12	75	45.00	1.5	0.605	0.61
13	75	60.00	0.5	0.383	0.35
14	50	30.00	1.5	0.531	0.48
15	100	60.00	1.5	0.576	0.62
16	50	45.00	0.5	0.003	0.076
17	75	30.00	2.5	0.893	0.93



is a rapid decrease in IONP formation after the first 3 h of incubation, and then a continued decline which is not demonstrated at 37 °C or 65 °C. Although the absorbance for IONP production is highest at 65 °C, the increasing absorbance after 5–6 h could be due to the aggregation of accumulated IONPs. At high temperatures, the reaction kinetics proceed rapidly, not allowing for proper growth during crystallization, leading to aggregation of larger particles (Pris, 2014).

The interplay between Fe^{3+} ions and bio-catalyst concentration result in nanoparticles of various morphologies and sizes and could be modulated to obtain size defined nanoparticles. Fig. 5c shows that an increase in ferric ion salt precursor concentration relates to an increase in rate of IONP generated within the same period of time. Higher concentrations of ferric ions contribute to an increased rate of primary particle formation during nucleation. This is depicted in Fig. 5c where increase in precursor concentration does not affect the time taken to reach peak absorbance but depicts an increase in yield of IONPs generated.

3.5. Optimization of external parameters using RSM

Although the OVAT analysis gives an overall illustration of the influence of external parameters on the optimal production of IONP, it lacks in accuracy in assessing the impact of the interaction of these parameters in this bioprocess. RSM gave a more accurate prediction and to determine the correlation between IONP yield with the 3 independent variables and the impact of interaction between these independent variables. 17 experimental runs were required for the Box-Behnken based experimental design which gave different responses depending on the combination of factors. Table 2 shows the experimental and predicted results obtained from the 17 runs using varying combinations of CFE concentration (A), temperature (B) and precursor concentration (C) as determined by the Box-Behnken experimental design.

The Stat-Ease Design Expert (Version 6.0) software was used to obtain analysis of variance (ANOVA) and regression coefficients for the mathematical model which was generated using multiple linear regression analysis of the 3 external parameters. This model represents the influence of all 3 independent variables and their interactive effect on IONP yield (Y). The values of the coefficient X_i , X_{ij} and X_{ijk} represent the independent effect of each variable on the response Y while coefficients with more than one factor depict the interactive effect. The influence on interactions between independent variables on IONP generation rate could be explained by the negative or positive value of the interactive coefficient which implies antagonistic and synergistic effects respectively (Mohamedin A. et al., 2015). All data was fitted to the quadratic polynomial model using backward elimination.

Statistical evidence of a high Fisher's model F-value ($F = 68.71$) and Prob < F ($p < 0.0001$) value from Table 3 confirm the significance of the model which is further validated by the insignificant lack of fit data ($p = 0.0841$) and R^2 value of 0.9888 which demonstrated that 98.88% of the total variability could be explained by the model. Reliability of the experimental design was also confirmed with the relatively lower coefficient of variation ($CV = 7.92$) which attests to the precision of the model. Model coefficients were calculated using multiple regression analysis with $p < 0.05$ values indicating the statistical significance of each coefficient. The second order polynomial equation that depicts the correlation between the dependent and independent variables and could be used in the prediction of optimal IONP generation rate is illustrated in equation 3:

Fig. 6. 3D response surface plots showing interaction between variables on IONP production. (a) precursor concentration (C) and temperature (B) (b) temperature (B) and CFE (A) (c) precursor concentration (C) and CFE (A).

$$Y(\text{IONP generation}) = 0.61 - 0.014A + 0.083B + 0.37C - 0.01A^2 + 0.047B^2 - 0.11C^2 - 0.098AB - 0.063AC - 0.082BCE$$

From Table 3, an evident statistical significance is displayed on model linear regression coefficients, B ($p = 0.014$) and C ($p < 0.0001$) and MS2 mediated generation of IONP. A strong interactive influence is also observed for parameters AB ($p = 0.0037$) and BC ($p = 0.0093$) and mild interactive influence of AC (0.0301) on IONP yield. All interactions are represented by negative regression coefficients, postulating an antagonistic interaction between these parameters on optimal generation of IONP.

The relationship between independent and dependent variables was graphically represented by 3D response surface plots which illustrate the interactive effects of two variables within their stipulated ranges with all other independent variables fixed at their medium value. With a 3D response surface plot, the influence of each factor on IONP generation rate is clearly visualized. Fig. 6a depicts the interaction between precursor concentration (C) and temperature (B) on MS2 mediated IONP yield. With the CFE concentration fixed at 50%, an increase in precursor concentration from 0.5 mM to 2.5 mM together with a decrease in temperature from 60 °C to 30 °C demonstrated an increase in IONP yield, confirming the antagonistic interaction between these variables. Fig. 6b shows that at 30 °C, an increase in CFE concentration from 50% to 100% showed an increase in IONP yield, suggesting that at 30 °C, an increase in the concentration of the bio-reducing agent (CFE) increased IONP yield. However, at 60 °C, an increase in CFE concentration from 50% to 100% showed a gradual decline in IONP yield. This could be because although the concentration of bio-reducing agent in the CFE increased, it could lose its stability at 60 °C and therefore decrease its Fe^{3+} reduction potential, resulting in lower IONP yield. With the temperature fixed at 45 °C, the interaction between CFE concentration and precursor concentration is demonstrated in Fig. 6c shows the effect of the interaction of precursor concentration and CFE concentration on optimal generation of IONP. From Fig. 6c, it is evident that precursor concentration exerts a strong effect on IONP generation because IONP yield increases with the increase of precursor concentration from 0.5 mM to 2.5 mM. However, CFE concentration does not demonstrate a strong influence on IONP generation. As the CFE concentration increases from 50 to 100% a drop in IONP generation is

observed. IONP yield is highest at CFE concentration of 50% and 2.5 mM precursor. This could be because at 50% CFE concentration, the production of the bio-reducing molecular could have reached a maximum and any further increase in CFE concentration would not generate more. However, an increase in precursor concentration contributes to the availability of Fe^{3+} ions for reduction, explaining the increase in IONP production. A numerical optimization carried out with the Design Expert software is shown in Table 5.

From Table 4, the solutions proposed through the BBD in RSM for optimal generation of MS2 mediated IONP was at a temperature of 55.75 °C, precursor concentration of 2.46 mM and CFE concentration of 55.58% which coincided with the findings of the OVAT analysis and RSM. The results of this RSM can further be projected to a sequential multi-step upscaling process where MS2 is inoculated and grown in 500 ml, 1 L, 5 L and 10 L shake flasks and then transferred to lab scale fermenters under the same growth conditions for industrial scale production.

Very few microbial processes have been reported in the optimization of the extracellular generation of IONP. Most of it are anaerobic processes (Moon et al., 2010; Byrne et al., 2015), necessitating the need for specialized equipment and N_2 air stream to maintain an anaerobic environment. Furthermore, extracellular bioprocesses are usually depicted to generate low rate of IONP formation (Rajendran and Sen, 2016) and yield. The results in this study reiterate that this MS2 aerobic bioprocess is an alternative, cleaner, one-step route for the production of stable IONPs without the use of capping or stabilizing agents. The underlying innovation

Table 5

Solutions proposed for optimal generation of MS2 mediated IONP using a numerical optimization method in RSM.

Solution No.	CFF	Temperature	Concentration	Response
1	55.58	55.75	2.46	1.00941
2	55.19	55.05	2.46	1.00411
3	51.23	52.26	2.49	1.00065
4	52.10	52.73	2.50	1.00398
5	50.11	54.35	2.47	1.02407
6	64.33	59.99	2.49	1.00313
7	50.19	57.67	2.29	1.0288
8	50.00	44.54	2.50	0.946113
9	50.00	60.00	1.79	0.942239
10	54.30	30.00	2.50	0.903641

Table 4

Analysis of variance of coefficient estimation for polynomial quadratic model in RSM depicting microbial mediated IONP fabrication under 3 independent variables.

ANOVA for Response Surface Quadratic Model						
Source	Coefficient Estimation	Sum of Squares	Mean Squares	F Value	DF	Prob > F
Model		1.31	9	0.15	68.71	<0.0001
Intercept	0.61			1		
A	−0.014	1.540E−003	1	1.540E−003	0.72	0.4228
B	0.083	0.056	1	0.056	26.17	0.0014
C	0.37	1.12	1	1.12	527.23	<0.0001
A2	−0.010	4.532E−004	1	4.532E−004	0.21	0.6582
B2	0.047	5.131E−003	1	5.131E−003	4.4	0.0741
C2	−0.11	0.047	1	0.047	22.31	0.0021
AB	−0.098	0.039	1	0.039	18.17	0.0037
AC	−0.063	0.016	1	0.016	7.35	0.0301
BC	−0.082	0.027	1	0.027	12.66	0.0093
Residual	0.015		72.125E−003			
Lack of Fit	0.012		33.866E−003	4.71	0.0841	
Std. Deviation	0.046	R-Squared		0.9888		
Mean	0.58	Adj R-Squared		0.9744		
C.V.	7.92	Pred R-Squared		0.8565		
PRESS	0.19	Adeq Precision		26.381		

lies in manipulating the microbial metabolic tolerance mechanisms to high levels of Fe^{3+} to generate nanostructures of commercial significance. This coincides with the aims of cleaner production in the conversion of an industrial waste (iron) into a value added product that can be carried out with low energy requirements unlike physical methods such as high energy ball milling, laser ablation and vapour deposition. This bioprocess has been shown to perform well at low temperatures (25–30 °C) and demonstrates ease of scale-up. This is because the mathematical model derived in RSM could be modulated to determine parameter requirements at a higher scale. Additionally, compared to chemical synthesis, MS2 generated IONPs lack residual surface toxicants and remain stable for over a week without stabilizers or capping agents. The byproducts generated as waste in this bioprocess are minimal and biodegradable, thus not posing a threat to the environment. Also, the optimization of this bioprocess using RSM was crucial to determine the statistical significance of the influence of selected process parameters on IONP generation and yield and instrumental in multi-stage sequential scale up operations (Ranjan, A.P. et al., 2012) for industrial scale production using this cleaner production method.

4. Conclusion

We describe here a microbial biosystem as an alternative route to IONP synthesis by exploiting its heavy metal tolerance metabolic mechanism to generate a value-added product. Unlike other green processes, MS2 generation of IONPs performed well at 35 °C and with low precursor concentrations of 1.0 mM, without the aid of specialized equipment, thereby not imposing high energy and equipment investment. The kinetics study found that nanoparticle generation commenced after 10 min and reached its maximum rate of production within 3 h of the commencement of the reaction, reinforcing its high rate of production and also remained stable for more than 7 days without a capping agent.

This microbial bioprocess to generate IONP which was innovated by exploiting the metabolic mechanism of the novel *Streptomyces* strain to tolerate and breakdown high levels of heavy metals such as Fe^{2+} has proved to be a clean process that could be fine-tuned for rapid, large scale generation of mono-dispersed, size defined iron oxide nanoparticles. Also, MS2 growth requirements were at minimal cost, with no specific media or energy requirements, with the generated IONPs remaining stable over a 48 h period without the addition of stabilizers or capping agents. It is therefore postulated that this process could pave an alternative pathway for industrial scale cost effective production of well-designed and stable IONPs.

Acknowledgements

The author would like to acknowledge Universiti Putra Malaysia for provisions of research funding using the VOT No. 9582100 under the Geran Putra Scheme.

References

Abenojar, Eric C., Wickramasinghe, Sameera, Bas-Concepcion, Jesbaniris, Samia, Anna Cristina S., 2016. Structural effects on the magnetic hyperthermia properties of iron oxide nanoparticles. *Prog. Nat. Sci.: Mater. Int.* 26 (5), 440–448. <https://doi.org/10.1016/j.pnsc.2016.09.004>, 1002–0071.

Adelere, I., Lateef, A., 2016. A novel approach to the green synthesis of metallic nanoparticles: the use of agro-wastes, enzymes, and pigments. *Nanotechnol. Rev.* 5, 567–587.

Ahmad, Razi, Mohsin, Mohd, Ahmad, Tokeer, Sardar, Meryam, 2015. Alpha amylase

assisted synthesis of TiO_2 nanoparticles: structural characterization and application as antibacterial agents. *J. Hazard. Mater.* 283, 171–177. <https://doi.org/10.1016/j.jhazmat.2014.08.073>, 0304–3894.

Apte, M., Girmé, G., Nair, R., Bankar, A., Kumar, A.R., Zinjarde, S., 2013. Melanin mediated synthesis of gold nanoparticles by *Yarrowia lipolytica*. *Mater. Lett.* 95, 149–152. <https://doi.org/10.1016/j.matlet.2012.12.087>.

Byrne, J.M., Muhamadali, H., Coker, V.S., Cooper, J., Lloyd, J.R., 2015. Scale-up of the production of highly reactive biogenic magnetite nanoparticles using *Geobacter sulfurreducens*. *J. R. Soc. Interface* 12 (107), 20150240. <https://doi.org/10.1098/rsif.2015.0240>.

Couto, Diana, Freitas, Marisa, Carvalho, Félix, Fernandes, Eduarda, 2015. Iron oxide nanoparticles: an insight into their biomedical applications. *Curr. Med. Chem.* 22, 1808–1828. <https://doi.org/10.2174/0929867322666150311151403>.

Dong, C. N., Tate, J.A., Kett, W.C., Batra, J., Demidenko, E., Lewis, L.D., 2015. Tumor cell targeting by iron oxide nanoparticles is dominated by different factors in vitro versus in vivo. *PLoS One* 10 (2), e0115636. <https://doi.org/10.1371/journal.pone.0115636>.

Fu, Fenglian, Dionysiou, Dionysios D., Liu, Hong, 2014. The use of zero-valent iron for groundwater remediation and wastewater treatment: a review. *J. Hazard. Mater.* 267, 194–205. <https://doi.org/10.1016/j.jhazmat.2013.12.062>, 0304–3894.

Jacob, Patricia, Masarudin, Jaffri, Hussein, Mohd, Abdul Rahim, Raha, 2017. Facile aerobic construction of iron based ferromagnetic nanostructures by a novel microbial nanofactory isolated from tropical freshwater wetlands. *Microb. Cell Factories* 2017 (16), 175. <https://doi.org/10.1186/s12934-017-0789-3>.

Jayashree, J., Nilotpal, P., Dash, B.P., Panda, P.K., Mishra, B.K., 2015. Pigment mediated biogenic synthesis of silver nanoparticles using diatom sp. and its antimicrobial activity. *J. Saudi Chem. Soc.* 19 (6), 661–666. <https://doi.org/10.1016/j.jscs.2014.06.005>, 1319–6103.

Kumar, B., Smita, K., Angulo, Y., Cumbal, L., 2016. Green synthesis of silver nanoparticles using natural dyes of cochineal. *J. Clust. Sci.* 27, 703–713. <https://doi.org/10.1007/s10876-016-0973-3>.

Lateef, A., Adelere, I.A., Gueguim-Kana, E.B., Asafa, T.B., Beukes, L.S., 2015. Green synthesis of silver nanoparticles using keratinase obtained from a strain of *Bacillus safensis* LAU 13. *Int. Nano Lett.* 5, 29–35. <https://doi.org/10.1007/s40089-014-0133-4>.

Lin, X.M., Samia, A.C., 2006. Synthesis, assembly and physical properties of magnetic nanoparticles. *J. Magn. Magn. Mater.* 305 (1), 100–109.

Moon, J.-W., Rawn, C.J., Rondinone, A.J., Love, L.J., Roh, Y., Everett, S.M., Phelps, T.J., 2010. Large-scale production of magnetic nanoparticles using bacterial fermentation. *J. Ind. Microbiol. Biotechnol.* 37 (10), 1023–1031.

Ohkoshi, S.-i., Namai, A., Yoshikiyo, M., Imoto, K., Tamazaki, K., Matsuno, K., Inoue, O., Ide, T., Masada, K., Goto, M., Goto, T., Yoshida, T., Miyazaki, T., Angew., 2016. Multimetal-substituted epsilon-iron oxide $\epsilon\text{-Ga}_{0.31}\text{Ti}_{0.05}\text{Co}_{0.05}\text{Fe}_{1.59}\text{O}_3$ for next-generation magnetic recording tape in the big-data era. *Chem. Int. Ed.* 55, 11403. <https://doi.org/10.1002/ange.201604647>.

Oves, M., Saghir Khan, M., Huda Qari, A., Nadeen Felemban, M., Almeelbi, T., 2016. Heavy metals: biological importance and detoxification strategies. *J. Biorem. Biodegrad.* 7, 334. <https://doi.org/10.4172/2155-6199.1000334>.

Pris, M., 2014. Influence of Different Parameters on Wet Synthesis of Silver Nanoparticles. Bachelor's thesis, University of Twente.

Rajendran, K., Sen, S., 2016. Optimization of process parameters for the rapid biosynthesis of hematite nanoparticles. *J. Photochem. Photobiol., B: Biology* 159, 82–87.

Saif, S., Tahir, A., Chen, Y., 2016. Green synthesis of iron nanoparticles and their environmental applications and implications. *Nanomaterials* 6 (11), 209. <https://doi.org/10.3390/nano6110209>.

Shen, Zheyu, Wu, Aiguo, Chen, Xiaoyuan, 2017. Iron oxide nanoparticle based contrast agents for magnetic resonance imaging. *Mol. Pharm.* 14 (5), 1352–1364. <https://doi.org/10.1021/acs.molpharmaceut.6b00839>.

Teymourian, Hazhir, Abdollah Salimi, Khezrian, Somayeh, 2013. Fe_3O_4 magnetic nanoparticles/reduced graphene oxide nanosheets as a novel electrochemical and bioelectrochemical sensing platform. *Biosens. Bioelectron.* 49, 1–8. <https://doi.org/10.1016/j.bios.2013.04.034>, 0956–5663.

Turick, C.E., Tisa, L.S., Caccavo Jr., F., 2002. Melanin production and use as a soluble electron shuttle for Fe(III) oxide reduction and as a terminal electron acceptor by *Shewanella algae* BrY. *Appl. Environ. Microbiol.* 68 (5), 2436–2444. <http://doi.org/10.1128/AEM.68.5.2436-2444.2002>.

Wahajuddin, Arora, S., 2012. Superparamagnetic iron oxide nanoparticles: magnetic nanoplateforms as drug carriers. *Int. J. Nanomed.* 7, 3445–3471. <http://doi.org/10.2147/IJN.S30320>.

Wang, Y., Aisen, P., Casadevall, A., 1995. *Cryptococcus neoformans* melanin and virulence: mechanism of action. *Infect. Immun.* 63 (8), 3131–3136. PMID: 7622240.

Wu, W., He, Q., Jiang, C., 2008. Magnetic iron oxide nanoparticles: synthesis and surface functionalization strategies. *Nanoscale Res. Lett.* 3 (11), 397.

Zheng, Huaijin, Chatfield, Christa, Liles, Mark, Cianciotto, P., Nicholas, 2013. Secreted pyomelanin of *Legionella pneumophila* promotes bacterial iron uptake and growth under iron-limiting conditions. *Infect. Immun.* 81 (11), 4182. <https://doi.org/10.1128/IAI.00858-13>.